# High-Order Mimetic Finite-Difference Operators Satisfying the Extended Gauss Divergence Theorem

Johnny Corbino, Jose E. Castillo

*Computational Science Research Center, 5500 Campanile Drive, San Diego, CA 92182*

**Abstract**

We present high-order mimetic finite-difference operators that satisfy the extended Gauss theorem. These operators have the same order of accuracy in the interior and at the boundary, no free parameters and optimal bandwidth. They are defined over staggered grids, using weighted inner products with a diagonal norm. We present several examples to demonstrate that mimetic finite-difference schemes using these operators produce excellent results.

*Keywords:* mimetic, finite-difference, differential operators, high-order

## 1. Introduction

Mimetic finite-difference methods have been experiencing a great deal of development in the last 10 years [1, 2, 3, 4, 5]. Many applications of these methods have been reported in the literature [6, 7, 8, 9, 10]. High-order mimetic finite-differences can be traced back to the work of Kreiss and Scherer [11], where they presented the summation by parts method (SBP). From their work, it is known that the order of accuracy at the boundary cannot be increased, with standard inner products, on nodal grids. They constructed a high-order SBP operator, increasing the order of accuracy at the boundary, with a weighted inner product, on nodal grids. This operator was two orders less accurate at the

*Email addresses:* jcorbino@sdsu.edu (Johnny Corbino), jcastillo@sdsu.edu (Jose E. Castillo)

boundary than the interior of the domain. In 2003, Castillo and Grone (CG) [12] using weighted inner products and staggered grids, constructed high-order divergence and gradient mimetic finite-difference operators with the same order of accuracy in the interior as well as at the boundary. CG operators have been extended to higher dimensions [13], and have been used successfully in several applications [14, 15, 16, 17, 18, 19]. However, these discrete operators have a set of free parameters and not necessarily the optimum bandwidth. In this paper, we construct high-order mimetic finite-difference operators divergence and gradient, on staggered grids, with diagonal weight matrix norms, no free parameters and optimal bandwidth. Tests comparing the CG operators with the ones presented, clearly show that the new operators produce better results.

This paper is organized as follows: In Section 2, we give a brief description of mimetic operators and staggered grids. In Section 3, we explain how to construct the one-dimensional second-order mimetic gradient, and present the fourth-order mimetic gradient and divergence. In Section 4, we describe how to compute the weight matrices for the inner products. In Section 5, we show how to construct the operators in higher dimensions using Kronecker products, we also introduce the mimetic laplacian and curl operators. Section 6, shows how these operators can be represented in a compact form, minimizing the size of the stencils. In Section 7, we present examples that clearly demonstrate that the new operators produce better results. Finally, our conclusions are provided in Section 8.

## 2. Mimetic operators

Mimetic operators, divergence ($\mathbf{D} \equiv \nabla\cdot$), gradient ($\mathbf{G} \equiv \nabla$), curl ($\mathbf{C} \equiv \nabla\times$) and laplacian ($\mathbf{L} \equiv \nabla^2$) satisfy the following vector calculus identities:

$$\mathbf{G}f_{const} = 0, \tag{1}$$

$$\mathbf{D}\nu_{const} = 0, \tag{2}$$

$$\mathbf{CG}f = 0, \tag{3}$$

$$\mathbf{DC}\nu = 0, \tag{4}$$

$$\mathbf{DG}f = \mathbf{L}f. \tag{5}$$

In addition, while providing an uniform order of accuracy, CG operators satisfy:

$$\langle \mathbf{D}\nu, f\rangle_Q + \langle \mathbf{G}f, \nu\rangle_P = \langle \mathbf{B}\nu, f\rangle \tag{6}$$

eq. (6) is the discrete analogue of the *extended Gauss divergence theorem* [13]. $\mathbf{B}$ is called the *mimetic boundary operator*, and it is obtained from:

$$\begin{aligned}
\langle Q\mathbf{D}\nu, f\rangle + \langle P\mathbf{G}f, \nu\rangle &= \langle \mathbf{B}\nu, f\rangle, \\
\langle Q\mathbf{D}\nu + \mathbf{G}^T P\nu, f\rangle &= \langle \mathbf{B}\nu, f\rangle, \\
Q\mathbf{D}\nu + \mathbf{G}^T P\nu &= \mathbf{B}\nu, \\
Q\mathbf{D} + \mathbf{G}^T P &= \mathbf{B}.
\end{aligned} \tag{7}$$

CG mimetic operators are defined over staggered grids. In this type of grids, scalar variables are stored at the centers of the cells; while vector components are placed at the edges (or faces, in 3D).

In the following figures, $m, n$ and $o$ represent the number of cells along the x-, y- and z-axes, respectively.

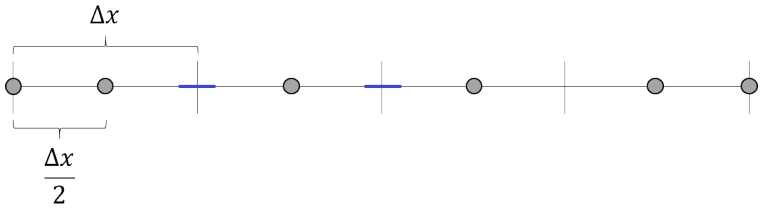


Figure 1: One-dimensional, uniform staggered grid. $m = 4$.

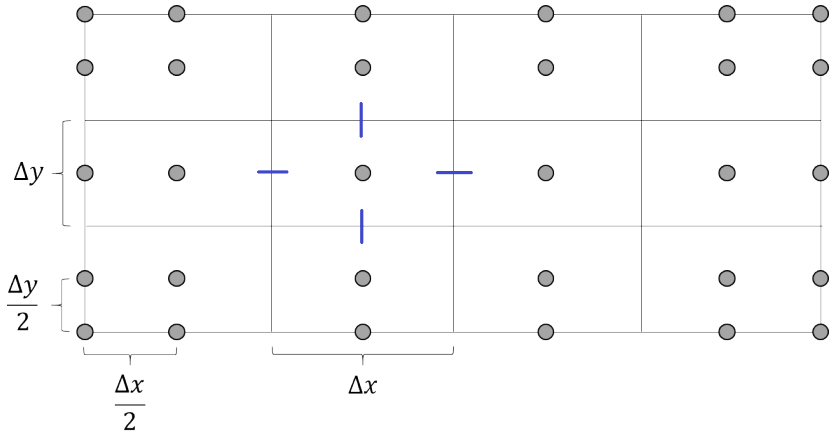


Figure 2: Two-dimensional, uniform staggered grid. $m = 4$ and $n = 3$.

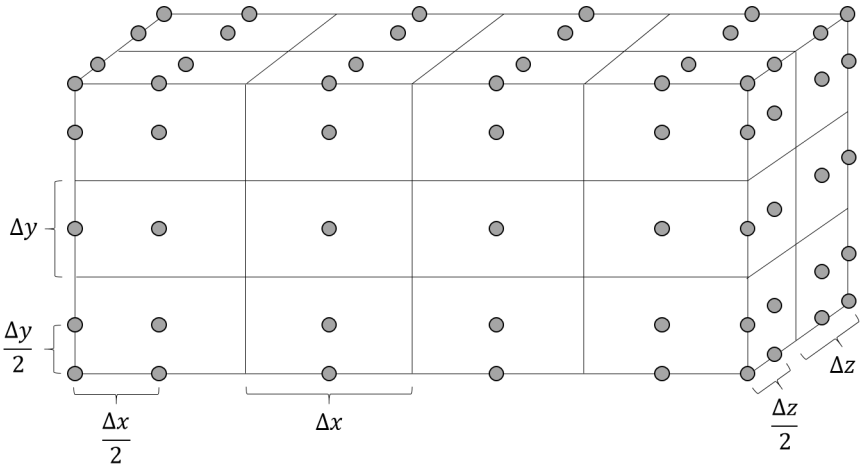


Figure 3: Three-dimensional, uniform staggered grid. $m = 4, n = 3$ and $o = 2$.

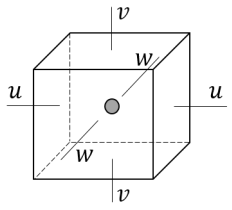


Figure 4: A 3D cell. $u, v$ and $w$ are the vector components used to compute the divergence. In case of the curl, we use the components that are tangential to the faces of the cell.

## 3. 1D operators

This section is focused on the construction of one-dimensional mimetic gradient and divergence operators.

One-dimensional operators can be visualized as follows:

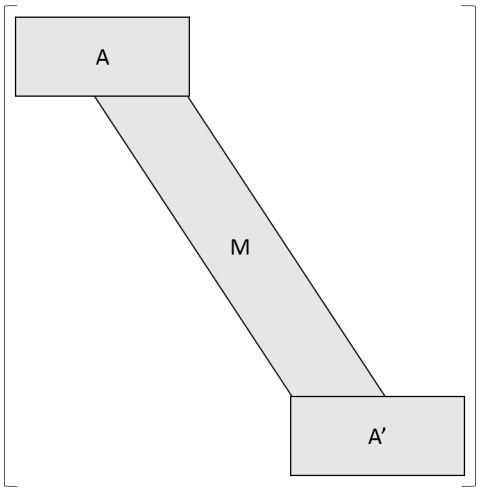


Figure 5: Taxonomy of 1D operators.

In fig. 5, $A$ and $A'$ are submatrices that approximate the derivatives at the left, and at the right boundary, respectively. $Dim(A) = Dim(A')$, and $A'$ is a permutation of $A$. $M$ is a banded matrix of width $k$ (order of accuracy) that approximates the derivative at the inner cells. The dimensions of $A$ depend on the type of operator and the desired order of accuracy. Details about these submatrices are provided in the following subsections.

### *3.1. Gradient*

To construct a *kth*-order mimetic gradient operator we need at least $2k$ cells ($m \geq 2k$) so that there is no overlapping between $A$ and $A'$.

$A$ and $A'$ will have dimensions $\frac{k}{2}$ by $k+1$. We proceed to construct a Vandermonde matrix from the stencil,

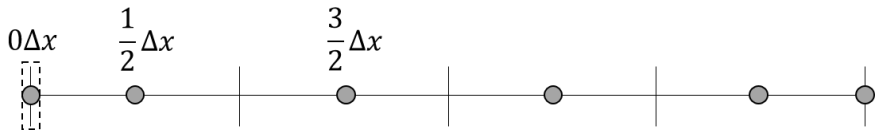


Figure 6: Stencil to compute a 2nd-order mimetic gradient at the left boundary. The segmented rectangle on the left represents the location of the value being calculated.

then, our "generator" vector is:

$$\begin{bmatrix} 0 & \frac{1}{2} & \frac{3}{2} \end{bmatrix}, \tag{8}$$

and the corresponding Vandermonde matrix,

$$\begin{bmatrix} 0 & \frac{1}{4} & \frac{9}{4} \\ 0 & \frac{1}{2} & \frac{3}{2} \\ 1 & 1 & 1 \end{bmatrix}, \tag{9}$$

Finally, we construct a right-hand side vector that only contains a '1' aligned to the second to last row of the matrix, producing the following system of linear equations:

$$\begin{bmatrix} 0 & \frac{1}{4} & \frac{9}{4} \\ 0 & \frac{1}{2} & \frac{3}{2} \\ 1 & 1 & 1 \end{bmatrix} \begin{bmatrix} x_1 \\ x_2 \\ x_3 \end{bmatrix} = \begin{bmatrix} 0 \\ 1 \\ 0 \end{bmatrix}. \tag{10}$$

and from the solution $[x_1, x_2, x_3] = \left[\frac{-8}{3} \quad 3 \quad \frac{-1}{3}\right]$, we obtain the first row of our matrix $A$. To obtain the successive rows of $A$ we just need to "shift" the stencil to the right $\frac{k}{2} - 1$ times.

and is computed as follows:

$$A' = -P_p A P_q \tag{11}$$

where, $P_p$ and $P_q$ are permutation matrices (flipped identity matrices) with dimensions $\frac{k}{2}$ by $\frac{k}{2}$ and $k+1$ by $k+1$, respectively. To construct the submatrix $M$ we use a centered stencil,


Figure 7: Inner stencil for 2nd-order mimetic gradient. Again, the segmented rectangle represents the location of the value being calculated.

70 which produces the following system:

$$\begin{bmatrix} \frac{-1}{2} & \frac{1}{2} \\ 1 & 1 \end{bmatrix} \begin{bmatrix} x_1 \\ x_2 \end{bmatrix} = \begin{bmatrix} 1 \\ 0 \end{bmatrix}, \tag{12}$$

and from the solution $[x_1, x_2] = [-1 \;\; 1]$, we obtain the rows of $M$. Putting all together we get:

$$\mathbf{G} = \frac{1}{\Delta x} \begin{bmatrix} \frac{-8}{3} & 3 & \frac{-1}{3} & & & \\ & -1 & 1 & & & \\ & & \ddots & \ddots & & \\ & & & -1 & 1 & \\ & & & \frac{1}{3} & -3 & \frac{8}{3} \end{bmatrix}_{(m+1),(m+2)} . \tag{13}$$

eq. (13) is the *2nd*-order one-dimensional mimetic gradient. For higher orders, our resulting gradient operators differ from CG. Here we present our *4th*-order $\mathbf{G}$:

$$\mathbf{G} = \frac{1}{\Delta x} \begin{bmatrix} \frac{-352}{105} & \frac{35}{8} & \frac{-35}{24} & \frac{21}{40} & \frac{-5}{56} & 0 & \cdots \\ \frac{16}{105} & \frac{-31}{24} & \frac{29}{24} & \frac{-3}{40} & \frac{1}{168} & 0 & \cdots \\ 0 & \frac{1}{24} & \frac{-9}{8} & \frac{9}{8} & \frac{-1}{24} & 0 & \cdots \\ \vdots & 0 & \ddots & \ddots & \ddots & \ddots & \end{bmatrix}_{(m+1),(m+2)} \tag{14}$$

in eq. (14), we show only the set of rows necessary to illustrate the overall structure of the matrix.

### *3.2. Divergence*

To construct a *kth*-order mimetic divergence operator we need at least $2k+1$ cells ($m \geq 2k+1$) so that there is no overlapping between $A$ and $A'$.

The methodology to construct a mimetic divergence is the same used to construct the mimetic gradient; except that $A$ and $A'$ will have dimensions $\frac{k}{2} - 1$ by $k+1$.

As before, we first exhibit the *2nd*-order operator,

$$\mathbf{D} = \frac{1}{\Delta x} \begin{bmatrix} 0 & \cdots & & & \\ -1 & 1 & & & \\ & \ddots & \ddots & & \\ & & -1 & 1 & \\ & & \cdots & 0 & \end{bmatrix}_{(m+2),(m+1)} \tag{15}$$

Notice that the first and last rows of eq. (15) are zero, this is because on one hand, the divergence does not have a physical meaning at the boundary nodes, and on the other hand, formula eq. (6) needs $D$ and $G$ to be compatible matrices under addition, and $G^T$ is $(m+2)$ by $(m+1)$, while $D$ without "augmentation", is $m$ by $(m+1)$. Our resulting divergence operators differ from CG when $k \geq 4$. Here is our *4th*-order $\mathbf{D}$:

$$\mathbf{D} = \frac{1}{\Delta x} \begin{bmatrix} 0 & \cdots & & & & & \\ \frac{-11}{12} & \frac{17}{24} & \frac{3}{8} & \frac{-5}{24} & \frac{1}{24} & 0 & \cdots \\ \frac{1}{24} & \frac{-9}{8} & \frac{9}{8} & \frac{-1}{24} & 0 & \cdots & \\ 0 & \ddots & \ddots & \ddots & \ddots & \ddots & \end{bmatrix}_{(m+2),(m+1)} \tag{16}$$

again, in eq. (16) we present only the set of rows necessary to illustrate the overall structure of the matrix.

## 4. Weight matrix P

The diagonal weight matrix $P$ (from eq. (6)) is obtained by:

$$\mathbf{G}^T p = b_{m+2}, \tag{17}$$

where $p$ is the main diagonal of $P$, and $b_{m+2}$ is the desired column sum $[-1 \ \cdots \ 0 \ \cdots \ 1]^T$.

For a *2nd*-order $\mathbf{G}$, the solution is $p = [\frac{3}{8} \ \ \frac{9}{8} \ \cdots \ 1 \ \cdots \ \frac{9}{8} \ \ \frac{3}{8}]^T$. System eq. (17) is overdetermined but consistent. For our *4th*-order $\mathbf{G}$ (and $m = 20$), we get:

$$p = \left[\frac{227}{641} \ \frac{941}{766} \ \frac{811}{903} \ \frac{1373}{1348} \ \frac{1401}{1400} \ \frac{36343}{36342} \ \frac{943491}{943490} \ 1 \ \cdots\right]^T. \tag{18}$$

### *4.1. Weight matrix Q*

The same procedure is applied to get matrix $Q$ (also from eq. (6)),

$$\mathbf{D}^T q = b_{m+1}, \tag{19}$$

system eq. (19) is also overdetermined but consistent, and has solution $q = \overrightarrow{1}$ for a *2nd*-order $\mathbf{D}$. In case of our *4th*-order $\mathbf{D}$ (and $m = 20$), we get:

$$q = \left[1 \ \frac{2186}{1943} \ \frac{1992}{2651} \ \frac{1993}{1715} \ \frac{649}{674} \ \frac{699}{700} \ \frac{18170}{18171} \ \frac{471744}{471745} \ 1 \ \cdots\right]^T. \tag{20}$$

Neither set of weights ($p$ or $q$) must be recomputed for a different number of cells; however, the number of '1s' in the middle increases proportionally with $m$.

## 5. 2D and 3D operators

In this section we explain how to construct higher-dimensional operators using the ones from section 3 and Kronecker products.

To construct a two-dimensional gradient:

$$\mathbf{G}_{xy} = \begin{bmatrix} S_x \\ S_y \end{bmatrix}, \tag{21}$$

where,

$$S_x = \hat{I}_n^T \otimes \mathbf{G}_x, \tag{22}$$

$$S_y = \mathbf{G}_y \otimes \hat{I}_m^T. \tag{23}$$

$\mathbf{G}_x, \mathbf{G}_y$ are the one-dimensional mimetic gradient operators for $x$ and $y$, respectively. $\hat{I}_m$ denotes an "augmented" identity matrix (first and last rows are zero),

$$\hat{I}_m = \begin{bmatrix} 0 & \cdots & \\ 1 & & \\ & \ddots & \\ & & 1 \\ & \cdots & 0 \end{bmatrix}_{(m+2),m} \tag{24}$$

To construct a three-dimensional gradient:

$$\mathbf{G}_{xyz} = \begin{bmatrix} S_x \\ S_y \\ S_z \end{bmatrix}, \tag{25}$$

where,

$$S_x = \hat{I}_o^T \otimes \hat{I}_n^T \otimes \mathbf{G}_x, \tag{26}$$

$$S_y = \hat{I}_o^T \otimes \mathbf{G}_y \otimes \hat{I}_m^T, \tag{27}$$

$$S_z = \mathbf{G}_z \otimes \hat{I}_n^T \otimes \hat{I}_m^T. \tag{28}$$

Here, $\mathbf{G}_x, \mathbf{G}_y, \mathbf{G}_z$ are the one-dimensional mimetic gradient operators for $x, y$ and $z$, respectively.

To construct a two-dimensional divergence:

$$\mathbf{D}_{xy} = \begin{bmatrix} S_x & S_y \end{bmatrix}, \tag{29}$$

where,

$$S_x = \hat{I}_n \otimes \mathbf{D}_x, \tag{30}$$

$$S_y = \mathbf{D}_y \otimes \hat{I}_m. \tag{31}$$

$\mathbf{D}_x, \mathbf{D}_y$ are the one-dimensional mimetic divergence operators for $x$ and $y$, respectively.

To construct a three-dimensional divergence:

$$\mathbf{D}_{xyz} = \begin{bmatrix} S_x & S_y & S_z \end{bmatrix}, \tag{32}$$

where,

$$S_x = \hat{I}_o \otimes \hat{I}_n \otimes \mathbf{D}_x, \tag{33}$$

$$S_y = \hat{I}_o \otimes \mathbf{D}_y \otimes \hat{I}_m, \tag{34}$$

$$S_z = \mathbf{D}_z \otimes \hat{I}_n \otimes \hat{I}_m. \tag{35}$$

$\mathbf{D}_x, \mathbf{D}_y, \mathbf{D}_z$ are the one-dimensional mimetic divergence operators for $x, y$ and $z$, respectively.

One-, two- and three-dimensional laplacian operators are obtained by:

$$\mathbf{L}_x = \mathbf{D}_x \mathbf{G}_x, \tag{36}$$

$$\mathbf{L}_{xy} = \mathbf{D}_{xy} \mathbf{G}_{xy}, \tag{37}$$

$$\mathbf{L}_{xyz} = \mathbf{D}_{xyz} \mathbf{G}_{xyz}. \tag{38}$$

Given a three-dimensional vector field:

$$\mathbf{F} = U\mathbf{i} + V\mathbf{j} + W\mathbf{k}, \tag{39}$$

the curl is defined as,

$$\nabla \times \mathbf{F} = \begin{vmatrix} \mathbf{i} & \mathbf{j} & \mathbf{k} \\ \frac{\partial}{\partial x} & \frac{\partial}{\partial y} & \frac{\partial}{\partial z} \\ U & V & W \end{vmatrix} = \left(\frac{\partial W}{\partial y} - \frac{\partial V}{\partial z}\right)\mathbf{i} + \left(\frac{\partial U}{\partial z} - \frac{\partial W}{\partial x}\right)\mathbf{j} + \left(\frac{\partial V}{\partial x} - \frac{\partial U}{\partial y}\right)\mathbf{k}, \tag{40}$$

we can express eq. (40) as,

$$\nabla \times \mathbf{F} = \left(\nabla \cdot \mathbf{F}^*_{yz}\right)\mathbf{i} + \left(\nabla \cdot \mathbf{F}^*_{zx}\right)\mathbf{j} + \left(\nabla \cdot \mathbf{F}^*_{xy}\right)\mathbf{k}, \tag{41}$$

where,

$$\mathbf{F}^*_{yz} = W\mathbf{j} - V\mathbf{k}, \tag{42}$$

$$\mathbf{F}^*_{zx} = U\mathbf{k} - W\mathbf{i}, \tag{43}$$

$$\mathbf{F}^*_{xy} = V\mathbf{i} - U\mathbf{j}. \tag{44}$$

therefore,

$$\mathbf{C}_{xy}\mathbf{F} = \left(\mathbf{D}_{xy}\mathbf{F}^*_{xy}\right)\mathbf{k}, \tag{45}$$

$$\mathbf{C}_{xyz}\mathbf{F} = \left(\mathbf{D}_{yz}\mathbf{F}^*_{yz}\right)\mathbf{i} + \left(\mathbf{D}_{zx}\mathbf{F}^*_{zx}\right)\mathbf{j} + \left(\mathbf{D}_{xy}\mathbf{F}^*_{xy}\right)\mathbf{k}. \tag{46}$$

are the two- and three-dimensional mimetic curls, respectively.

## 6. Compact operators

High-order ($k \geq 4$) mimetic operators can be represented in a "compact form" by factorizing the original matrices [20]. By doing this, we can attain higher orders of accuracy using a minimal stencil,

$$\mathbf{D}_{kth} = \mathbf{D}_{2nd} R_{kth}, \tag{47}$$

where $R_{kth}$ denotes the right factor matrix that when multiplied by the *2nd*-order divergence produces a *kth*-order $\mathbf{D}$ operator. The same can be done for the gradient,

$$\mathbf{G}_{kth} = L_{kth} \mathbf{G}_{2nd}, \tag{48}$$

the reason why we factorize the divergence from the right and the gradient from the left is because in this way we can express the laplacian operator as follows:

$$\mathbf{L}_{kth} = \mathbf{D}_{2nd} R_{kth} L_{kth} \mathbf{G}_{2nd}. \tag{49}$$

$\mathbf{L}_{kth}$ is our *kth*-order mimetic laplacian, and $R_{kth} L_{kth}$ is called the *star* operator ($\mathbf{S}$). $\mathbf{S}$ can be seen as a tensor that contains properties that are inherent to each problem. In [21], the authors used compact representation of the CG operators to solve problems of acoustic wave propagation.

## 7. Accuracy tests

We performed several accuracy tests to compare our fourth order operators with those defined in [12]. In this section we show two of those tests,

$$F(x) = \log x + \cos x \tag{50}$$

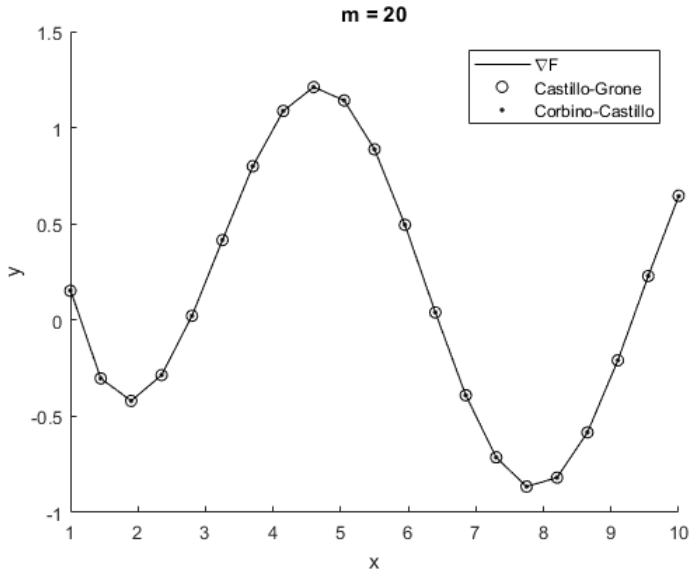


Figure 8: Comparison between continuous and discrete solutions. Visually, both discrete solutions look identical.

The following tables show the magnitude of the error obtained with each method (Castillo-Grone and Corbino-Castillo),

| Gradient | | | |
|---|---|---|---|
| $m$ | CG $\|E\|_2$ | CC $\|E\|_2$ | $(\Delta x)^4$ |
| 10 | 0.0915 | 0.0204 | 0.6561 |
| 20 | 0.0066 | 0.0047 | 0.0410 |
| 40 | 0.0019 | 8.7e-4 | 0.0026 |
| 80 | 2.6e-4 | 1.0e-4 | 1.6e-4 |

Table 1: Accuracy test for the gradient.

Comparing divergences...

| Divergence | | | |
|---|---|---|---|
| $m$ | CG $\|E\|_2$ | CC $\|E\|_2$ | $(\Delta x)^4$ |
| 10 | 0.0166 | 0.0174 | 0.6561 |
| 20 | 0.0018 | 0.0018 | 0.0410 |
| 40 | 4.4e-4 | 4.5e-4 | 0.0026 |
| 80 | 5.8e-5 | 5.9e-5 | 1.6e-4 |

Table 2: Accuracy test for the divergence.

Testing the laplacians with an elliptic problem,

$$\nabla^2 f(x) = e^x, \tag{51}$$

subject to:

$$\alpha f(0) - \beta f'(0) = 0, \tag{52}$$

$$\alpha f(1) + \beta f'(1) = 2e. \tag{53}$$

with $\alpha = 1$ and $\beta = 1$.

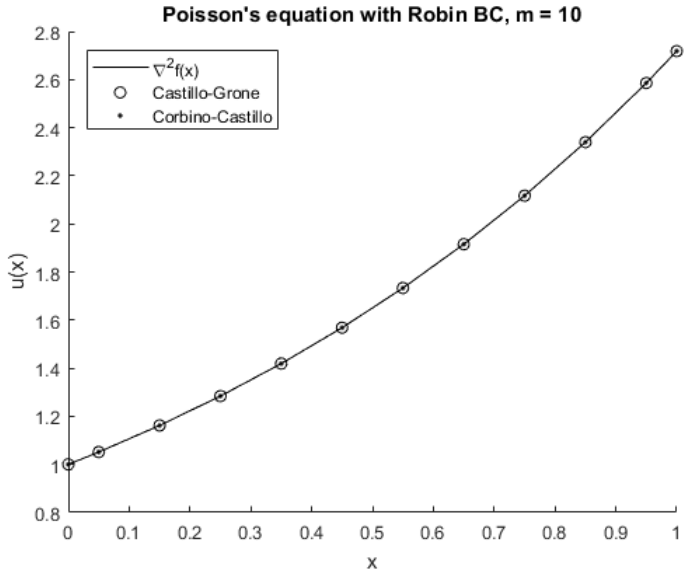


Figure 9: Solution to equation eq. (51). Both approximations look identical.

we obtained the following results:

| Laplacian | | | |
|---|---|---|---|
| $m$ | CG $\|E\|_2$ | CC $\|E\|_2$ | $(\Delta x)^4$ |
| 10 | 4.0e-5 | 1.2e-6 | 0.6561 |
| 20 | 4.3e-6 | 6.8e-8 | 0.0410 |
| 40 | 4.1e-7 | 9.5e-9 | 0.0026 |
| 80 | 3.8e-8 | 1.0e-9 | 1.6e-4 |

Table 3: Accuracy test for the laplacian.

As shown on table 3, the new mimetic laplacian operator is also considerably more precise than its CG counterpart (in some cases for up to two orders of magnitude).

These tests have been done using the *Mimetic Operators Library Enhanced* (MOLE) [22].

## 8. Conclusions

High-order mimetic finite-difference operators that satisfy the extended Gauss divergence theorem have been presented. These operators have the same order of accuracy in the interior and at the boundary, no free parameters and optimal bandwidth. They are constructed on staggered grids, using weighted inner products with a diagonal norm. Their construction using linear algebra illustrate the clarity of their formulation. A compact formulation, which uses the minimum second order stencils, has also been presented. These operators have been implemented in the open-source mathematical library MOLE. Mimetic finite-difference schemes using these operators produced excellent results on our test cases.

## References


[1] M. Shashkov, Conservative Finite-Difference Methods on General Grids, CRC Press, 1995.

[2] D. Batista, J. E. Castillo, Mimetic schemes on non-uniform structured meshes 34 (2009) 152–162.

[3] J. E. Castillo, M. Yasuda, Linear systems arising for second-order mimetic divergence and gradient discretizations 4 (2005) 67–82.

[4] J. E. Castillo, et al., Large sparse linear systems arising from mimetic discretization 53 (2007) 1–11.

[5] O. Montilla, et al., Matrix approach to mimetic discretizations for differential operators on non-uniform grids 73 (2006) 215–225.

[6] J. M. Guevara-Jordan, et al., Convergence of a mimetic finite difference method for static diffusion equation, Advances in Difference Equations.

[7] M. Abouali, J. E. Castillo, Solving poisson equation with robin boundary condition on a curvilinear mesh using high order mimetic discretization methods, Mathematics and Computers in Simulation 139 (2017) 23–36.

[8] L. B. D. Veiga, et al., The Mimetic Finite Difference Method for Elliptic Problems, 2014.

[9] J. Hyman, et al., Mimetic finite difference methods for diffusion equations 6.

[10] F. Solano-Feo, et al., A new mimetic scheme for the acoustic wave equation.

[11] H. O. Kreiss, G. Scherer, Finite element and finite difference methods for hyperbolic partial differential equations, Mathematical Aspects of Finite Elements in Partial Differential Equations (1974) 195–212.

[12] J. E. Castillo, R. D. Grone, A matrix analysis approach to higher-order approximations for divergence and gradients satisfying a global conservation law, Matrix Analysis and Applications 25 (1) (2003) 128–142.

[13] J. E. Castillo, G. F. Miranda, Mimetic Discretization Methods, CRC Press, 2013.

[14] J. E. Castillo, et al., High-order mimetic finite difference methods on nonuniform grids.

[15] O. Rojas, et al., Modelling of rupture propagation using high-order mimetic finite differences, Geophysical Journal International 172 (2008) 631–650.

[16] E. J. Sanchez, et al., Algorithms for higher-order mimetic operators (2015) 425–434.

[17] J. de la Puente, et al., Mimetic seismic wave modeling including topography on deformed staggered grids 79 (2014) 125–141.

[18] J. Blanco, et al., Tensor formulation of 3-D mimetic finite differences and applications to elliptic problems 45 (2016) 457–475.

[19] C. Bazan, et al., Mimetic finite difference methods in image processing, Computational and Applied Mathematics 30 (2011) 701–720.

[20] M. Abouali, J. E. Castillo, High-order compact Castillo-Grone's mimetic operators, CSRC, 2012.

[21] L. J. Cordova, et al., Compact finite difference modeling of 2-D acoustic wave propagation, Journal of Computational and Applied Mathematics 295 (2016) 83–91.

[22] J. Corbino, J. E. Castillo, MOLE: Mimetic Operators Library Enhanced: The open-source library for solving partial differential equations using mimetic methods, 2017.